



Graphene in Large Area Hole-Conductor Free Perovskite

Solar Cells

Rahul Patidar

Department of Physics, IISER Pune

Thesis Supervisor:

Dr. Anish Priyadarshi

Research Fellow, Energy Research Institute, NTU, Singapore

Prof. Subodh Gautam Mhaisalkar

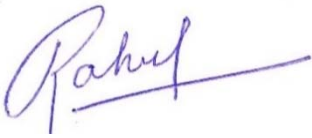
Department of Materials Science and Engineering, NTU, Singapore

Prof. Satishchandra B Ogale

Department of Physics, IISER Pune

CERTIFICATE

This is to certify that this dissertation entitled “Graphene in Large Area Hole Conductor Free Pervoskite Solar Cells” towards the partial fulfilment of the BS-MS dual degree programme at the Indian Institute of Science Education and Research, Pune represents study/work carried out by Rahul Patidar at Energy Research Institute @ NTU Singapore under the supervision of Professor Subodh Mhaisalkar, Professor Materials Science and Engineering and Executive-Director ERI@N during the academic year 2017-2018.




Rahul Patidar



Prof. Subodh Mhaisalkar

DECLARATION

I hereby declare that the matter embodied in the report entitled “**Graphene in Large Area Hole Conductor Free Pervoskite Solar Cells**” are the results of the work carried out by me at the Energy Research Institute, Nanyang Technological University, Singapore, under the supervision of Prof Subodh Mhaisalkar and the same has not been submitted elsewhere for any other degree.



Rahul Patidar



Prof. Subodh Mhaisalkar

ACKNOWLEDGEMENTS

First I would like to extend my sincere thanks to all my supervisors and start with Dr. Anish Priyadarshi, senior research fellow at Energy Research Institute, Nanyang Technological University (NTU) who was there to constantly guide me in my research. He has been a great leader and a great support throughout my thesis work. I would also like to extend my gratitude to Prof. Subodh Mhaisalkar from the department of Materials Science and Engineering at NTU who gave me an opportunity to work in his group and whose suggestions during the group meetings were very valuable and ensured a constant progress of this project. I would also like to thank Prof. Satish Ogale from the department of Physics, IISER Pune who have been a great inspiration to me to continue to give my best and excel at everything I do.

At last I would like to thanks my parents for making me a person I am today.

Content

1 Introduction.....	9
1.1 Background.....	9
1.2 Objective.....	11
2 Theory.....	12
2.1 Solar Irradiance.....	12
2.2 Photovoltaic Effect.....	12
2.3 Perovskite Material.....	13
2.4 Perovskite Solar Cells.....	14
2.5 Screen Printer	15
2.7 Solar Simulator	16
3 Methods.....	19
3.1 Characterization.....	19
3.1.1 Raman Spectroscopy.....	19
3.1.2 Photoluminescence Spectroscopy.....	20
3.1.3 Field Emission Scanning Electron Microscopy.....	20
3.2 Experimental.....	21
3.2.1 Fabrication of fully Printable PSCs.....	21
3.2.2 Graphene TiO ₂ Composite.....	22
4 Results and Discussion.....	23
5 Conclusion.....	30
6 References.....	31

List of Figures

Fig.1 Architecture of PSC.....	10
Fig.2 Architecture of Fully Printable Perovskite Solar Cells.....	11
Fig.3 Spectral Irradiance.....	12
Fig.4 Methyl Ammonium Lead Iodide Crystal Structure.....	13
Fig.5 Perovskite Solar Cells Working Principle.....	15
Fig.6 Screen Printer Schematic.....	16
Fig.7 Circuit representation of Solar Cells.....	17
Fig.8 IV Curve of a Solar Cell.....	17
Fig.9 Raman Spectrum of Single Layer Graphene.....	19
Fig.10 Schematic of Scanning Electron Microscopy.....	21
Fig.11 Printing of Perovskite Solar Cells.....	22
Fig.12 Graphene TiO ₂ Composite.....	23
Fig.13 Raman Spectrum of Graphene TiO ₂ Composite.....	23
Fig.14 SEM images of the device stack.....	24
Fig.15 Relative Performance of perovskite solar cells.....	25
Fig.16 Hysteresis in Perovskite Solar Cells.....	26
Fig.17 Charge Extraction in Perovskite Solar Cells.....	27
Fig.18 Electrochemical Impedance Spectra.....	28
Fig.19 Equivalent Circuit for Impedance Spectra Fit.....	28
Fig.20 Stability of Perovskite Solar Cells.....	29
Fig.21 Large Area Device.....	29

List of Tables

Table 1 Screen Printers Parameters for thickness variations.....	15
Table 2 Perovskite Solar Cells Performance Comparison.....	25
Table 3 Perovskite Solar Cells Performance Comparison for Large Area Device.....	29

Abstract

Carbon based hole conductor free fully printable perovskite solar cells (PSCs) has caught quite attention in the perovskite field since the introduction of the novel architecture in 2014. Thanks to the incredibly high stability of this device architecture compared to the standard gold based perovskite solar cells. TiO₂ has been typically used as an electron transport layer (ETL) in this type of architecture. Recently, graphene based ETLs has shown to be a good substitute to pristine TiO₂ to achieve higher conductivity and higher carrier injection leading to better performance. Here, we show the composite of graphene and TiO₂ as a promising ETL for more efficient and stable perovskite solar cells. The composite when used as an ETL shows improvement in current density and fill factor. Moreover, we also observe a drastic improvement in stability of these PSCs compared to the reference cells.

1. Introduction

There is no denying the fact that we need clean and renewable energy sources globally. At present, we draw most of the energy from fossil fuels which are non-renewable and require finite resources while contributing to the global warming as well. So, the need for cheap and renewable resources is greatly desired. An efficient and more feasible alternative option is solar energy. Solar energy has tremendous potential to meet world energy demands which is apparent from the fact that one hour of energy from sun can suffice the energy need of the world for a year. [1]

A variety of technology converts solar energy into usable energy for buildings. Solar photovoltaic is one of them, which uses solar radiation to generate electricity directly. While this technology has been widely disparaged for being expensive, the cost has considerably fallen in the last decade thanks to the advancement in technologies.

The current market leader of photovoltaic industry is silicon solar cells which has long life time of up to 20 years and are very efficient as well. However, high temperature processing and use of toxic materials like cadmium telluride and copper indium selenide in silicon photovoltaics makes them questionable for future energy demands. For this reasons, researchers have been exploring new materials and fabrication techniques which is more straightforward and requires less energy to process while bringing the cost further down. Organic photovoltaics (OPs) and Dye-sensitized solar cells (DSSCs) held a lot of promise as they can be transited into flexible, lightweight and low-cost power sources with more straightforward wet chemistry techniques. However, the power conversion efficiency of both DSSCs and OPs is far behind the traditional silicon solar cells due to their limited optical absorption and lower carrier mobility.

Recently, organo-metal halide perovskites have become largely popular owing to their facile processing and exceptional optoelectrical properties such as high optical absorption coefficient, direct bandgap long carrier lifetime and diffusion length making them an excellent light absorbing material for photovoltaic application[2-4]. Perovskite solar cells (PSC) have tremendously improved from power conversion efficiency (PCE) of 3% to 22.1% in just as short span of 5 years [5, 6]. Despite being cheaper than silicon solar cells and equivalently efficient, PSCs are still struggling to reach the market. The reason being the stability of PSCs. These cells are very sensitive and degrades rather quickly in presence of moisture, oxygen and UV. Therefore, scant efforts are needed in the direction of stable PSCs which is also the objective of this research work.

1.1 Background

The general device structure of PSC is shown in Fig.1. The layer of perovskite is sandwiched between hole transport material (HTM) and electron transport material (ETM). The light absorption takes place in the active

layer of perovskite material which leads to the generation of electron and hole pair. Electron and holes are then extracted by ETM and HTM respectively. Transparent conducting oxide (TCO), such as indium tin oxide (ITO) or fluorine doped tin oxide (FTO) is used as transparent electrode on top of glass while gold is usually used as the other electrode on top of HTM.

PSCs can be broadly classified in two types on the basis of their architecture, Mesoscopic PSCs and Planar PSCs. Mesoscopic PSCs consist of one mesoporous layer (usually it's TiO_2 or Al_2O_3) on top of compact ETM, the role of which is to provide scaffold for the growth of perovskite crystals. Whereas in the planar architecture all layers are compact. However, the difference in the performance of both architecture is not very significant and both have shown efficiency over 20%.

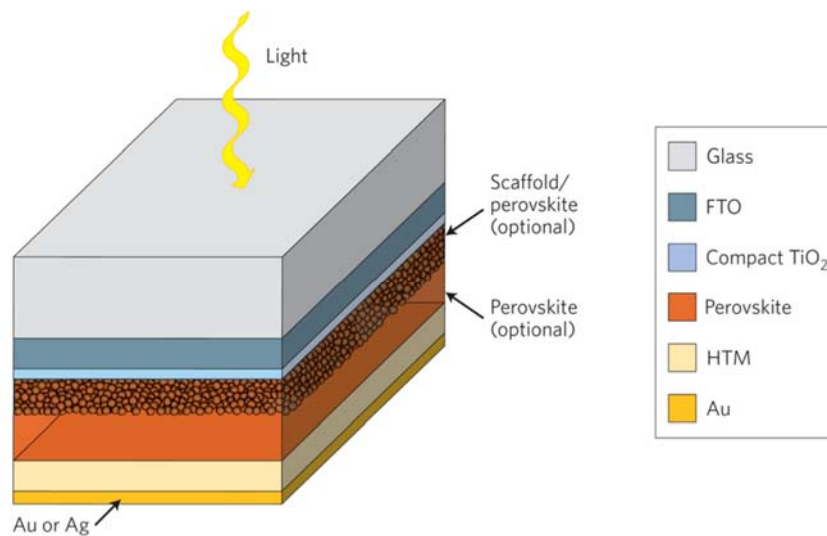


Fig. 1: Architecture of Perovskite Solar Cells[7].

The first PSCs, inspired from the design of DSSCs, replaced dye molecules with perovskite crystals[5]. However, owing to the instability of perovskite in the liquid iodide/iodine redox couple electrolyte led to the significantly lower performance. Later in 2012, the use of relatively stable 2,2,7,7-tetrakis-(N,Ndi-pmethoxyphenylamine) 9,9-bifluorene (spiro-OMeTAD) as a hole transport material (HTM) led to the improvement in the device performance[8, 9]. Advancing further many organic materials has been used as HTM. However, most organic HTMs are costly and sensitive to degradation in the presence of moisture and also are vulnerable to the migration of halide ions and metal ions (from metal contact). Using the large electron-hole diffusion length researchers have shown that perovskite can act as a light harvester and a charge transporter [2, 10-12]. These reports have facilitated HTM free PSCs [11, 12]. Since then many inorganic materials have been used for HTM free PSCs including Au, Ni and carbon [10, 13, 14]. Having good conductivity Au is used as the most efficient counter electrode, but it also increases the fabrication cost of solar cells and thus questioning the commercial

development. Contrary, carbon holds a lot of promise to be used as counter electrode thanks to the good conductivity, and abundance of the carbon in nature. However, the most thought-provoking properties that make carbon a frontrunner for the industrial needs are its inherent hydrophobic nature and inert to ion migration originating from perovskite and metal contact which leads to higher stability up to 2000h[15]. Planar carbon electrode based PSCs has been mostly focused and studied but because of the poor contact between carbon and perovskite and an uncontrollable thickness between the electron transport material and carbon contact limits the efficiency of the device. Addressing these issues, researchers developed high efficient hole conductor free fully printable mesoscopic perovskite solar cells (MPSCs), which employs a triple mesoporous layer of TiO_2 , ZrO_2 and carbon as a scaffold [Fig.2] and perovskite is infiltrated from the top of carbon as a light harvester [16]. ZrO_2 separates electron collecting material from carbon contact which can be accurately controlled. Being able to screen print these devices makes their fabrication process simpler and cheaper for them to reach the market.

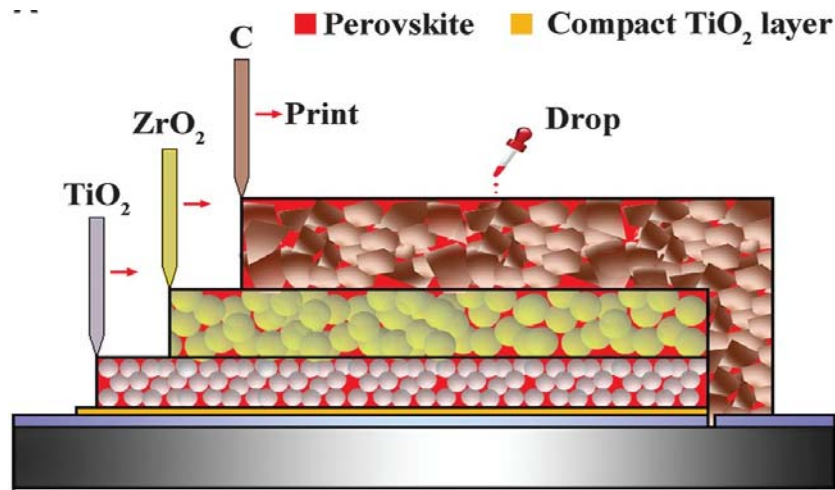


Fig. 2: Architecture of fully printable mesoscopic perovskite solar cells [16].

1.2 Objective:

The objective of this work is to understand the fabrication mechanism of large area fully printable PSC and incorporate graphene in the mesoporous architecture for the enhancement of efficiency and stability. Composite of TiO_2 and graphene has shown to improve the efficiency and stability of PSC[17]. The research work aims to reproduce the similar results in fully printable hole conductor free carbon devices.

2. Theory

2.1 Solar Irradiance

Electromagnetic waves received on earth ranges from 100nm to 1mm. Fig. 3 below is a diagram showing the distribution of solar energy across the electromagnetic spectrum received by Earth.

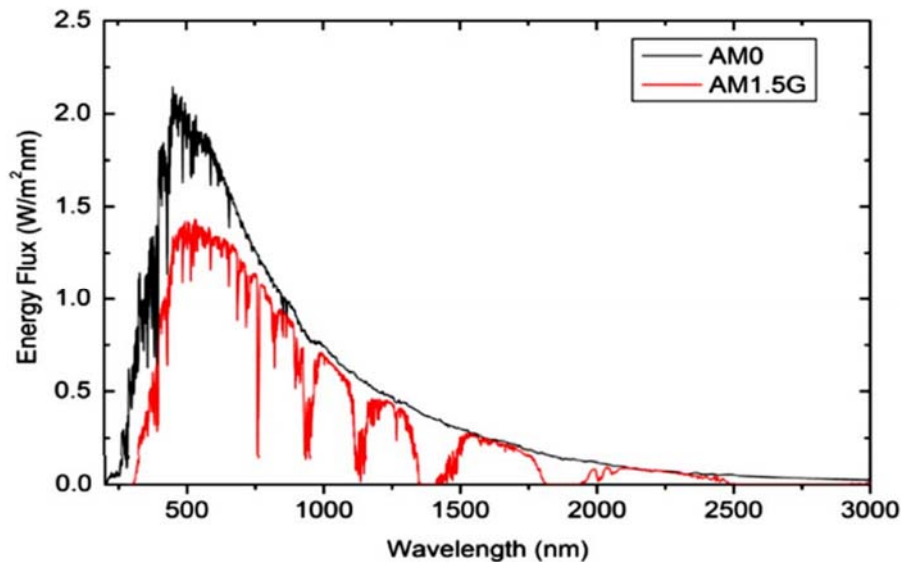


Fig. 3 Graph of Spectral Irradiance against wavelength [18]

The region delineated in black is the intensity of sunlight received at the top of the atmosphere, while the region demarcated by red is the direct solar irradiance intensity at sea level. The peak of the red region is lower due to the attenuation of the Sun rays as they pass through the atmosphere. There are also several dips in several regions of wavelengths which is mainly due to absorption from the gas molecules in the atmosphere. This red region is generally referred to as AM1.5G standard, which is commonly used in solar simulators to provide illumination which is as close as natural sunlight.

2.2 Photovoltaic effect

It was in 1839 when French Physicist A. E. Becquerel demonstrated the generation of an electric current by immersing two electrodes of platinum or gold in an acid, alkaline or neutral solution while exposing it to the solar irradiation, and the phenomena was called Becquerel Effect (now referred to as photovoltaic effect).

Electromagnetic radiation contains photons and each photons carries a specific amount of energy depending on the wavelength according to the following relation,

$$E = \frac{hc}{\lambda}$$

E is the energy of incident photon, c the representation for speed of electromagnetic wave in vacuum, and λ is wavelength of the photon.

A photon of energy equal or larger than the bandgap of material hits the material and excites an electron or the charge carrier to the higher energy state. The band gap is the difference between the energy of conduction band and valence band. It is also referred as HOMO-LUMO gap for organic semiconductors. HOMO stands for highest occupied molecular orbital (valence band) and LUMO stands for lowest unoccupied molecular orbital (conduction band). The separation of the generated electrons and holes is facilitated by inbuilt potential and are then collected by respective electrodes to produce the voltage. This phenomena of creation of voltage and current in a material upon exposure of light is known as photovoltaic effect.

2.3 Perovskite Material

The crystal structure of Calcium Titanium Oxide (CaTiO_3) is known as the perovskite structure. In 2009 metal halide perovskite was first used as dye in dye sensitized solar cells and had displayed PCE of 3.9%.[19]. The standard formula of metal halide perovskite is ABX_3 where B is the divalent metal cation, X is halide anion and A can be an organic or inorganic cation. The divalent metal cation B is located at the centre which is surrounded by halide ions located at face centre and cation A located on the corner of the lattice as shown in Fig.4.

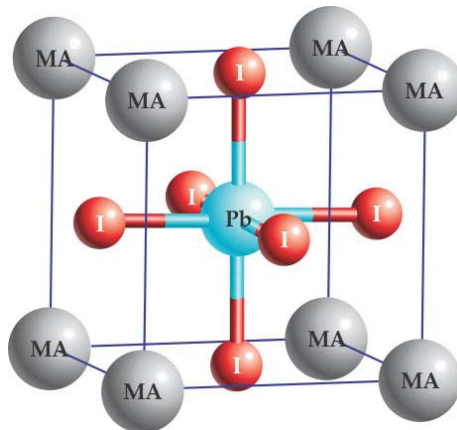


Fig.4: Crystal structure of Methyl ammonium lead triiodide perovskite[20]

Material with ABX_3 configuration can have various structure conditional to their anionic and cationic radii of X, A and B and also on the interaction of A cation with BX_6 . Goldschmidt tolerance factor (t) is the trustworthy

indicator for the stability and distortion of the perovskite crystals[21]. The Goldschmidt factor is defined using ionic radius of atoms as described in the following equation:

$$t = \frac{r_A + r_X}{\sqrt{2}(r_B + r_X)}$$

Where the radius of cation A is represented by r_A while r_B is the representation for the radii of cation B and r_X is the anionic radius of the halides. Overall, cubic lattice is preferred with the tolerance factor in the range of 0.9-1 whereas octahedral is formed in the range of 0.71-0.9 also called as distorted perovskite structure. When tolerance factor exceeds the value 1 or falls less than 0.71, non-perovskite structures are formed [21].

Organic-inorganic metal halide perovskite has been directly used in perovskite solar cells (PSC). Direct band gap, solution processability, high light absorption coefficient ($1.5 \times 10^4 \text{ cm}^{-1}$ at 550 nm), a long charge carrier diffusion length ($\sim 100 \text{ nm}$ for $\text{CH}_3\text{NH}_3\text{PbI}_3$ and $\sim 1 \mu\text{m}$ for $\text{CH}_3\text{NH}_3\text{PbI}_{3-x}\text{Cl}_x$), and high carrier mobility makes them an excellent choice for photovoltaic application [2, 4, 8]. Despite of these excellent optoelectronic properties, stability of halide perovskite is still a concern. The instability in presence of moisture, oxygen and UV are the most recognized degradation of perovskite materials and needs scant efforts for their commercial success.

2.4 Perovskite Solar Cell (PSC)

The schematic band diagram of PSC is shown in Fig.5. The light is shined from the glass side and is absorbed by perovskite layer generating excitations. Having low exciton energy of perovskite material, the excitons are separated to free electron and holes at room temperature. After the generation of free charge carriers electrons are transferred to transparent electrode via ETM while holes are transferred to metallic contact via HTM generating a potential equivalent to the work function difference of the two electrodes. If not separated, the generated electron and hole pair would recombine immediately to reach the minimum total energy of the system. Therefore, role of HTM and ETM is critical to avoid recombination and deliver maximum performance. The ideal ETM would have a conduction band slightly lower than that of perovskite to facilitate the transfer of electron and valence band significantly lower than that of perovskite to block the transfer of holes from perovskite to ETM. Similarly, ideal HTM would have valence band higher than that of perovskite to facilitate the transfer

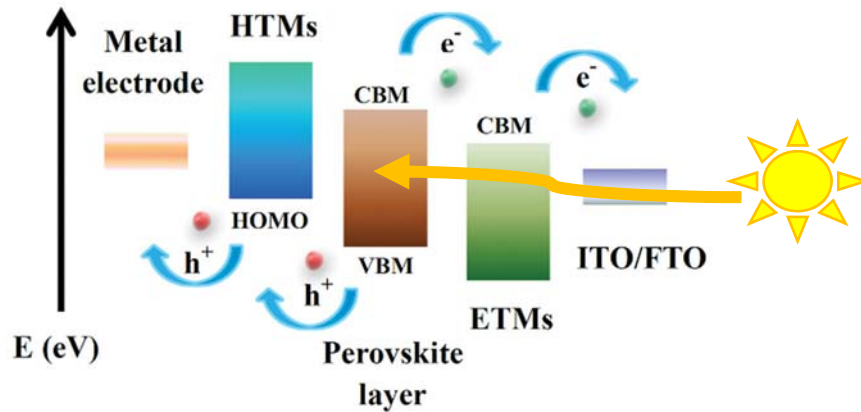


Fig. 5 Working principle of conventional PSC [22].

of holes while the conduction band should be significantly higher than that of perovskite to block the electrons to enter into HTM. However, still some of the electrons and holes may recombine before they reach the electrodes. It is mainly caused by interfacial defects in the device, and these defects will result in the drop of charge collection. This, in turn will have a negative effect on the current density (J_{sc}) and open circuit voltage (V_{oc}) of the solar cell.

2.5 Screen Printer

It is important to discuss the mechanism of screen printer as the whole fabrication of photovoltaic cells is carried out by this simple technology. This technology has been widely used in textile and electronics industries and has become widely popular owing to its simple operation which makes scaling the process significantly easier and cheaper. The screen printer functions by moving the squeegee across a screen with a mesh opening, which consequently squeezes the paste or ink through and onto the surface of the substrate. The screen printer used in this research work is semi-automated.

Variable	To achieve: Thicker film	To achieve: Thinner Film
Screen Thickness	Increase	Decrease
Emulsion Thickness	Increase	Decrease
Paste Viscosity	Increase	Decrease
Screen Gap	Increase	Decrease
Squeegee Speed	Increase	Decrease
Squeegee Pressure	Decrease	Increase

Table 1 Correlation of screen printer parameters with thickness of the printed film

The thickness of the film can be controlled by adjusting various parameters of screen printer listed in the table above. To obtain a consistent and uniform print, we chose to print with a slow squeegee speed and high squeegee pressure. Below is a table describing the required variation to achieve the desired thickness of a film.

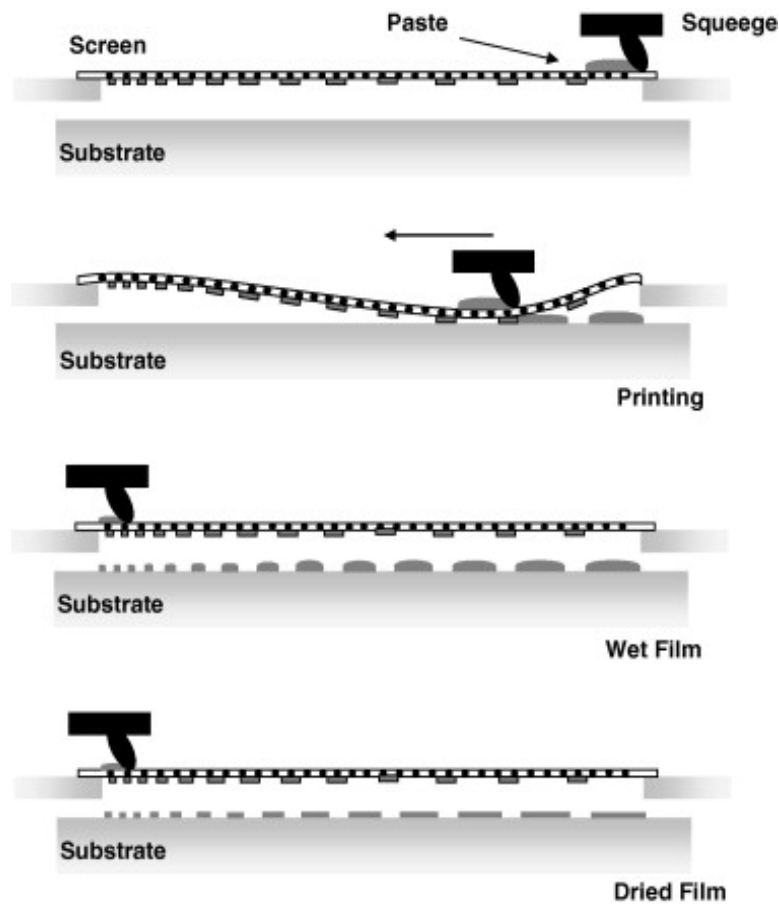


Fig. 6 Schematic illustration of Screen Printer[23]

2.6 Solar Simulator

Solar Simulator is a device that delivers the closest spectral match to the sun available from any light source using xenon lamp. The purpose of this machine is to produce similar environment as the outside environment under laboratory condition.

The solar radiation in outer space is more than what we receive at the earth surface, the reason being the absorption of radiation by the gases present in earth atmosphere. For the reasons above the universal air mass coefficient used for measuring solar cell is 1.5 AM. This gives the power of 1000 W/m^2 from the Sun with an atmospheric thickness of 1.5 due to the solar zenith angle of 48.2° . The source meter measures the current response over a voltage sweep and provides the J-V plot of the device. The J-V plot is then used to measure the open circuit voltage (V_{oc}), current density (J_{sc}), fill factor (FF) and efficiency (η) of a solar cell. All these parameters will be defined later in this section.

A typical solar cell can be demonstrated by a current source in a parallel connection with a diode. However, more realistic model would be with the addition of a shunt and series resistance. (Fig. 7)

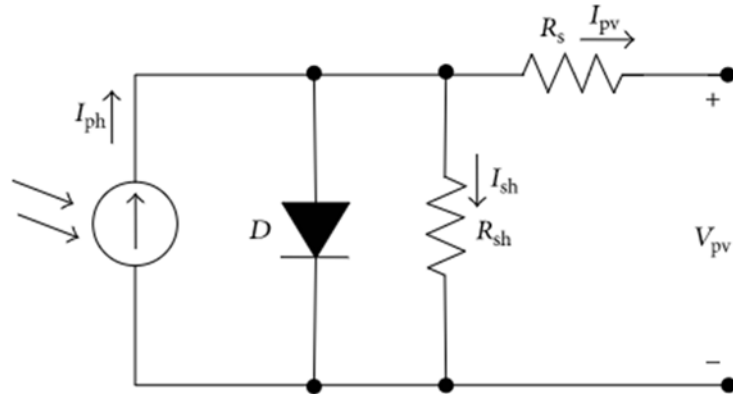


Fig. 7 Equivalent circuit representation of solar cell[24]

The current in a typical solar cell is equal to the photogenerated current subtracted by the current through the diode and is represented via the following equation,

$$I = I_L - I_0(e^{\frac{qv}{nkT}} - 1)$$

I is the total current from the solar cell, I_L is the photogenerated current by the cell while I_0 represents the saturation current of the internal diode, q is an elementary charge, V is applied or generated voltage, k and T is Boltzmann constant and absolute temperature respectively.

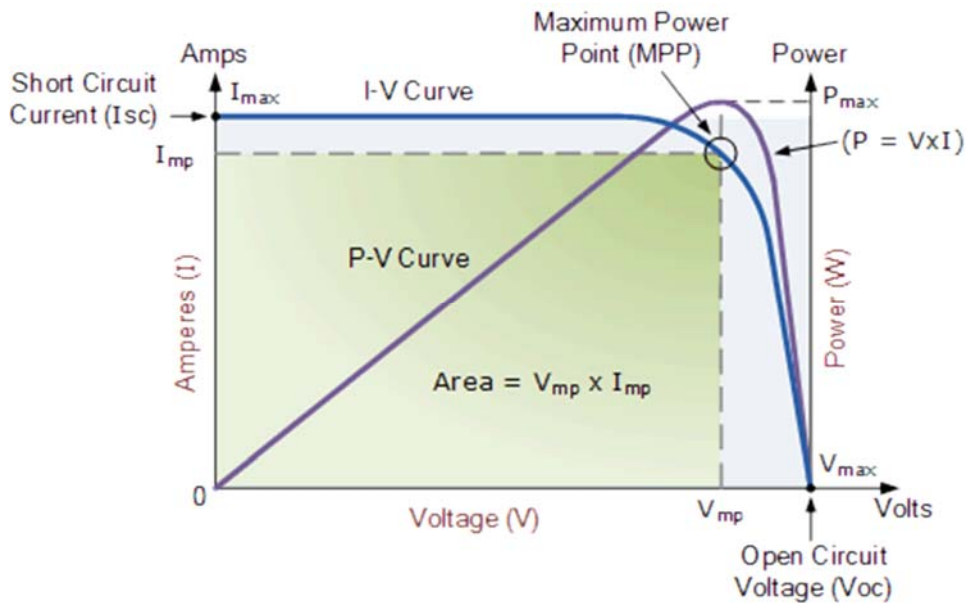


Fig.8 I-V curve of solar cell [25]

The power generated by a photovoltaic cell can be obtained by the multiplication of current and voltage.

$$P = IV$$

For a certain amount of irradiation the power curve is obtained by scanning the voltage across the operational window (Fig.8).

V_{oc} , open circuit voltage is the peak voltage produced by a photovoltaic cell and can be defined as the voltage produced under no load or zero current through the circuit. At the other extreme, when the circuit is closed, that is when anode and cathode are connected, the voltage recorded is zero. The current flowing through the cell at zero volt is known as short circuit current of solar cell, or I_{sc} . Of course, no power is generated on either of these two conditions, which means there must be a point somewhere in between zero and V_{oc} where the solar cell produces maximum power. Alternatively, the point of the photovoltaic cell at where it gives maximum power (green rectangle Fig. 8) is referred as the “maximum power point” or MPP. The current and voltage at this point are typically represented as I_{mp} and V_{mp} respectively. Therefore, the ideal working point of a photovoltaic cell is the maximum power point. However, MPP is not directly used as the parameter to characterize the performance of photovoltaic cell. The FF which stands for Fill Factor, determines the maximum power that can be generated by a solar cell. The FF is defined by the equation:

$$FF = \frac{V_{mp}I_{mp}}{V_{oc}I_{sc}}$$

The efficiency of the solar cell is the ratio of the output power with respect to the input power. P_{in} is the power of the incident irradiance. P_{out} can be replaced by P_{max} since the solar cell can be operated at its maximum power output to get the peak performance.

$$\eta = \frac{P_{out}}{P_{in}} \Rightarrow \eta = \frac{P_{max}}{P_{in}}$$

Efficiency also depends on other factors like wavelength and power of the incident radiation and also on the solar cell temperature. Therefore, precautions needs to be taken to accurately characterize and compare the performance between the devices.

3 Methods

In this section characterization and experimental techniques will be discussed which will include fabrication mechanism of perovskite solar cells and characterization of materials.

3.1 Characterization

The following sections will discuss the different characterization techniques used in this research work.

3.1.1 Raman Spectroscopy

One of the easy and fast ways to characterize graphene is via Raman Spectroscopy. Named after Indian physicist Sir C V Raman, this tool is used to detect vibrational, rotational and other low frequency modes in a system. It's a very useful technique to characterize Sp^2 and Sp^3 hybridized carbon atom and therefore is very suitable for materials like graphene, graphite, carbon nanotubes. Moreover, it can be very well used to differentiate multilayer graphene from single layer or double layer graphene and also the defects identification can be done using Raman spectra.

Raman spectra of single layer graphene is shown in Fig.9. The G-mode is at about $1587cm^{-1}$, a primary in plane vibrational mode and is attributed to the stretching of the C-C bond in graphitic materials, and can be observed in all sp^2 carbon systems.

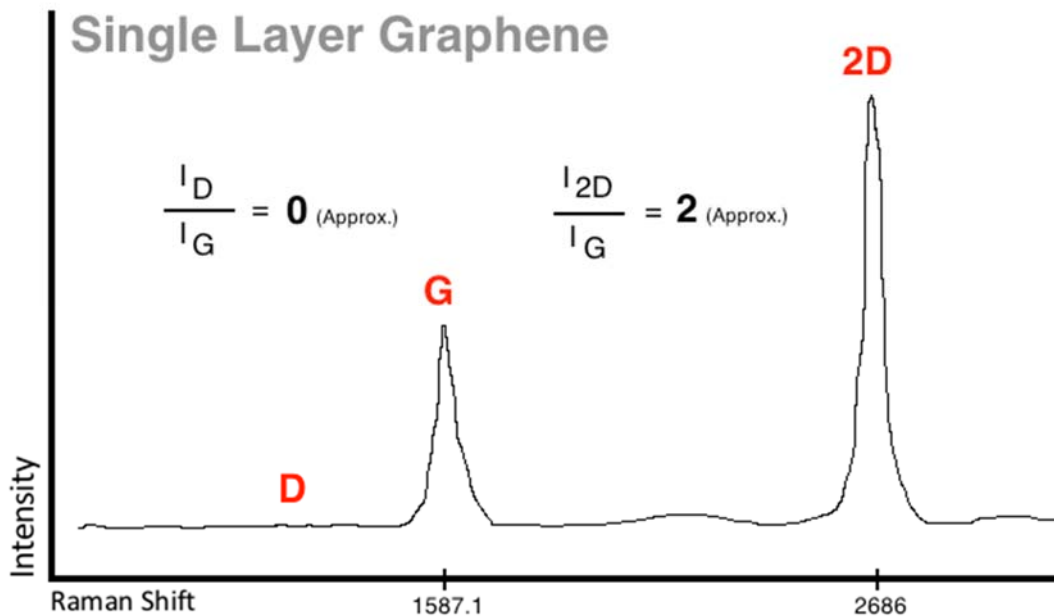


Fig.9 Raman spectra of single-layer graphene [26]

The presence of D band is credited to the defects in graphene. As can be seen in the figure above, no D peak is present in the Raman spectra of a single layer graphene indicating presence of no defects. The band in the range 2500 - 2800 cm^{-1} is called the 2D band. This band is present in all types of sp^2 carbon materials in the Raman spectra. Together with the G-band, the spectrum with 2D band is a Raman sign of the presence of graphitic sp^2 materials. Also, the Raman spectra can be used to calculate the number of layers of the graphene. For multi-layer graphene 2D band is usually broad while in the case of single-layer graphene it's quite intense and sharp.

3.1.2 Photoluminescence Spectroscopy

Photoluminescence (PL) Spectroscopy is a tool to probe the electronic structure of materials without having to destroy it. From the monochromatic light source, light hits the sample, where the photon excites the electron to the higher energy level in a process called photo-excitation. Return of the excited electron to the ground state releases the energy by emitting a photon. In the case of excitation via photon, the observed luminescence is called photoluminescence. The energy of the emitted photon tells the difference in energy levels between the higher energy state and the ground state. In the context of PSCs, PL is usually used to probe the charge extraction or charge transfer dynamics of a material. Quenching of PL is related to the charge extraction by the adjacent layer, more the quenching better the charge extraction is. Hence, PL is a great tool and commonly used to probe the charge extraction capability of HTM and ETM.

3.1.3 Field-emission Scanning Electron Microscope (FESEM)

FESEM is used in labs across all the discipline of science to image very small (upto 50nm) topographic details of the object. FESEM, as the name suggests, uses a beam of high energy electrons to image the object. The applied field causes the reduction in the work function of metal leading to the tunneling of electrons. Electrons are liberated within the high vacuum and accelerated in a high electrical field gradient. Emitted electrons are focussed to produce a narrow beam also referred as primary beam that bombards the object. Secondary electrons, the electrons reflected from each spot on the object are collected at the detector and an electronic signal is produced. The angle and velocity of these secondary electrons determines the surface morphology of the object. The signal is then amplified and converted to a digital image that can be seen on the computer.

In Material Science, FESEM is a very useful tool to observe the morphology of the material which allows you to tailor them according to the experimental need.

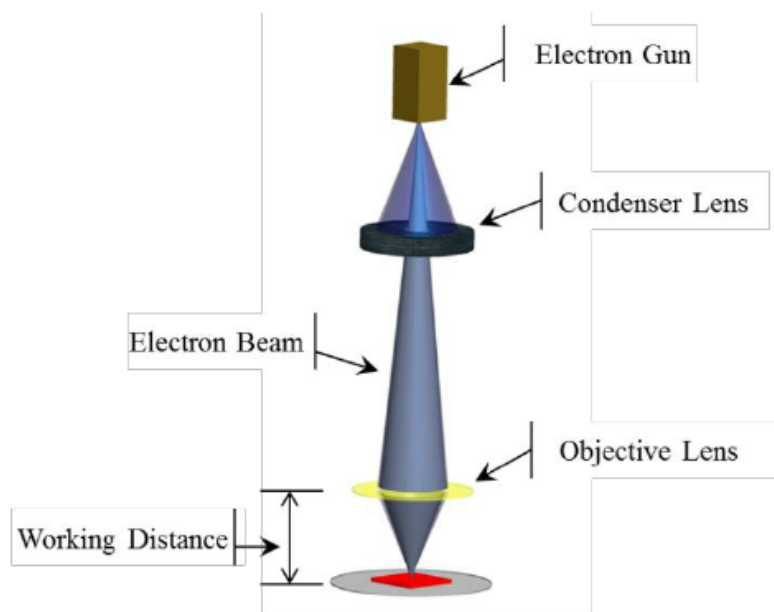


Fig. 10 Schematic of a basic SEM [27]

3.2. Experimental

3.2.1 Fabrication of Fully Printable Perovskite Solar Cells

Laser-patterned fluorine-doped tin oxide (FTO) glass was ultrasonically cleaned with soap solution, deionized water, and ethanol sequentially. Chemical bath technique was used to deposit an initial seed layer of TiO_2 onto the FTO substrate. The solution of TiCl_4 was diluted to 50mM using DI water, and the substrate was immersed for 30mins at 70°C . After cleaning with DI water substrates were sintered at 500°C for 30mins. Following which, a thin layer (50nm) of blocking layer (Dyesol BL1) was screen printed and sintered at 500°C for 30mins. After cooling down, the substrate undergoes the final round of TiCl_4 bath treatment at 100mM for 30mins at 70°C to remove any pinholes instigated by the removal of organic binder from blocking layer. Once more, the substrate was sintered at 500°C for 30mins. The deposition of the mesoporous TiO_2 layer was done by using a diluted TiO_2 paste (Dyesol NRD 30). Dilution was done with terpineol in the weight ratio of 1:1.4 to achieve an optimized thickness of 450nm. Post printing of mesoporous TiO_2 , the substrates were fired at 500°C for 30mins to remove the organic binder. The ZrO_2 spacer layer was printed with an optimized thickness of 1.4 μm . The ZrO_2 paste (Zr-Nanoide ZT/SP) is used as it is. After printing, the substrate undergoes annealing process at 500°C for 30mins. The carbon paste (Dyesol) was used for the printing of the carbon contact and was fired at 400°C for 30mins with the optimized thickness of 10-15 μm .

Perovskite was synthesized by taking the equimolar ratio of PbI_2 and $\text{CH}_3\text{NH}_3\text{I}$ (Tokyo Chemical Limited, TCI) in GBL (γ -Butyrolactone Sigma, $\geq 99\%$). To control the crystallization kinetics, 5 AVA-I was added to the perovskite precursors in a molar ratio of 20:1 (MAI to AVA-I). The solution was stirred overnight at 50°C to make sure the complete dissolution of all the precursors. At the final step, perovskite precursor solution was drop casted on top of the carbon layer using pipette. For the devices with an active area of 0.7 cm^2 , $3.5\ \mu\text{L}$ of perovskite precursor solution was used. The complete process is described in Fig.11.

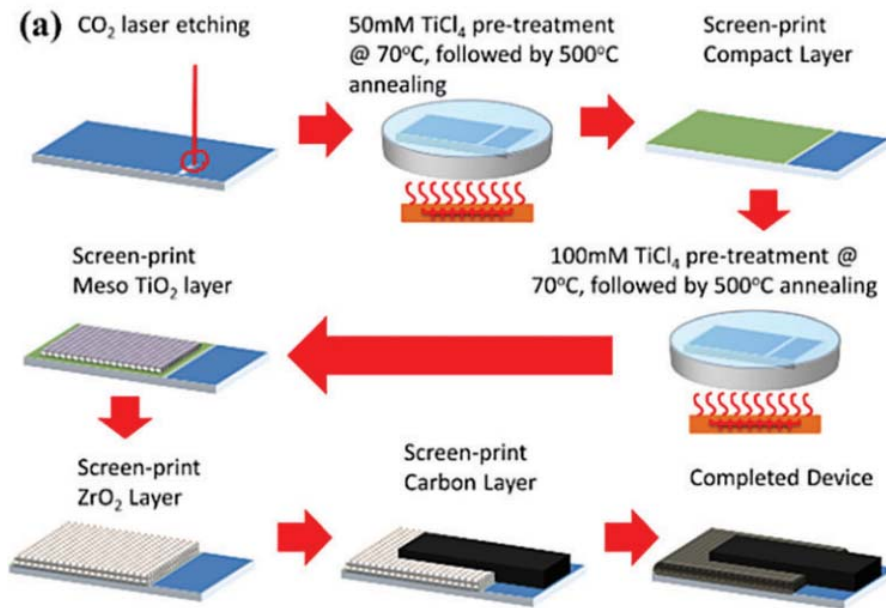


Fig 11 Schematic showing the complete fabrication process of PSCs[15]

Graphene TiO₂ composite was used in place of pristine TiO₂ in the device fabrication of graphene incorporated devices.

3.2.2 Graphene TiO₂ Composite

Powdered multilayer graphene was obtained from 2D center NUS. The obtained graphene was dispersed in dimethylformamide (DMF) with the ratio 1mg/ml followed by sonication for 1 hour. The dispersion was centrifuged at 11000 rpm for 30 minutes to remove the big flakes, and the supernatant was collected by pipetting. 10g of terpineol was added to the graphene dispersion and was stirred for half an hour. Terpineol being highly viscous and a high boiling point solvent; it is most suitable solvent for screen printing. Therefore, the solvent exchange was performed to switch from DMF to terpineol for the better printing of the composite. Exploiting the big difference between the boiling point of DMF and terpineol (which also justifies the use of DMF for the graphene dispersion) the solvent exchange was done using rotary evaporator. The rotary evaporator was set to 30 mbar at 80°C for 2 hours to remove DMF completely from the dispersion.

After the rotary evaporation, final dispersion of graphene in terpineol was obtained. To make the graphene TiO₂ composite the TiO₂ paste (Dyesol NRD 30) was mixed with the graphene dispersion in the ratio of 1:1.8 by weight. The obtained mixture was then kept for stirring overnight and was sonicated for 2 hours before using it for the fabrication of devices.

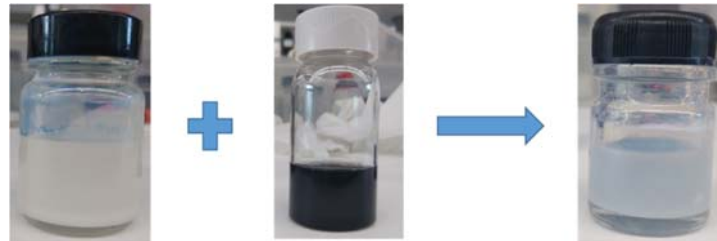


Fig. 12 Picture of TiO₂ before addition of graphene and after addition

4 Results and Discussion

The graphene/TiO₂ composite was characterized by Raman Spectroscopy to understand the quality of graphene in the composite. In a typical Raman spectrum of graphene, the G band correspond to the in-plane vibrational mode involving Sp² hybridized carbon atoms of graphene while the D peak has been attributed to the presence of defects in the system. [28] As shown in Fig. 13, the low intensity of D peak shows the presence of less defects in the composite. The ratio of the intensity of 2D band to the G band was calculated to be 0.61 while the value of the same ratio is 2 for the pristine single layer graphene. This shows that the majority of the graphene sheets in the composite are multi-layer graphene.

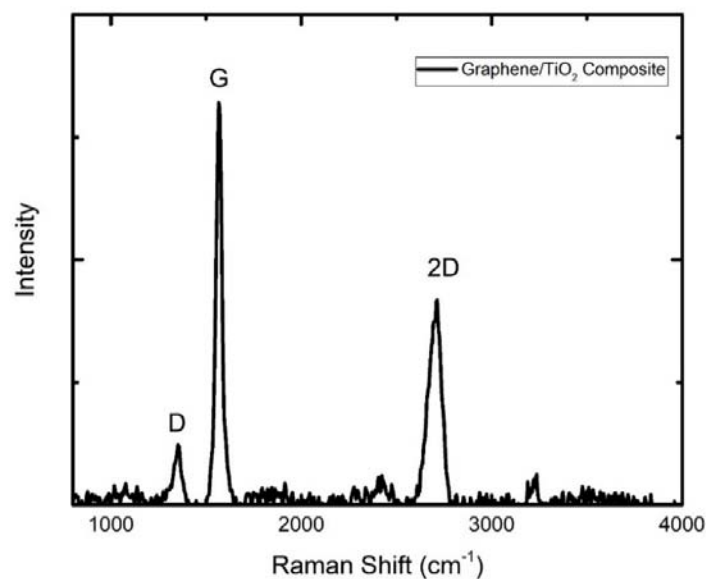


Fig. 13 Raman Spectrum of Graphene/TiO₂ composite.

To check any morphological changes in perovskite crystal growth in presence of graphene we performed cross section SEM of reference cells and the cells with graphene, with and without infiltrating perovskite. (Fig. 14). No morphological change was observed in the graphene/TiO₂ composite compared to pristine TiO₂ (Fig. 4a and 4b). Fig 4c and 4d are the images of complete device stack with infiltration of perovskite. As can be seen in the images no change in perovskite crystal growth was seen.

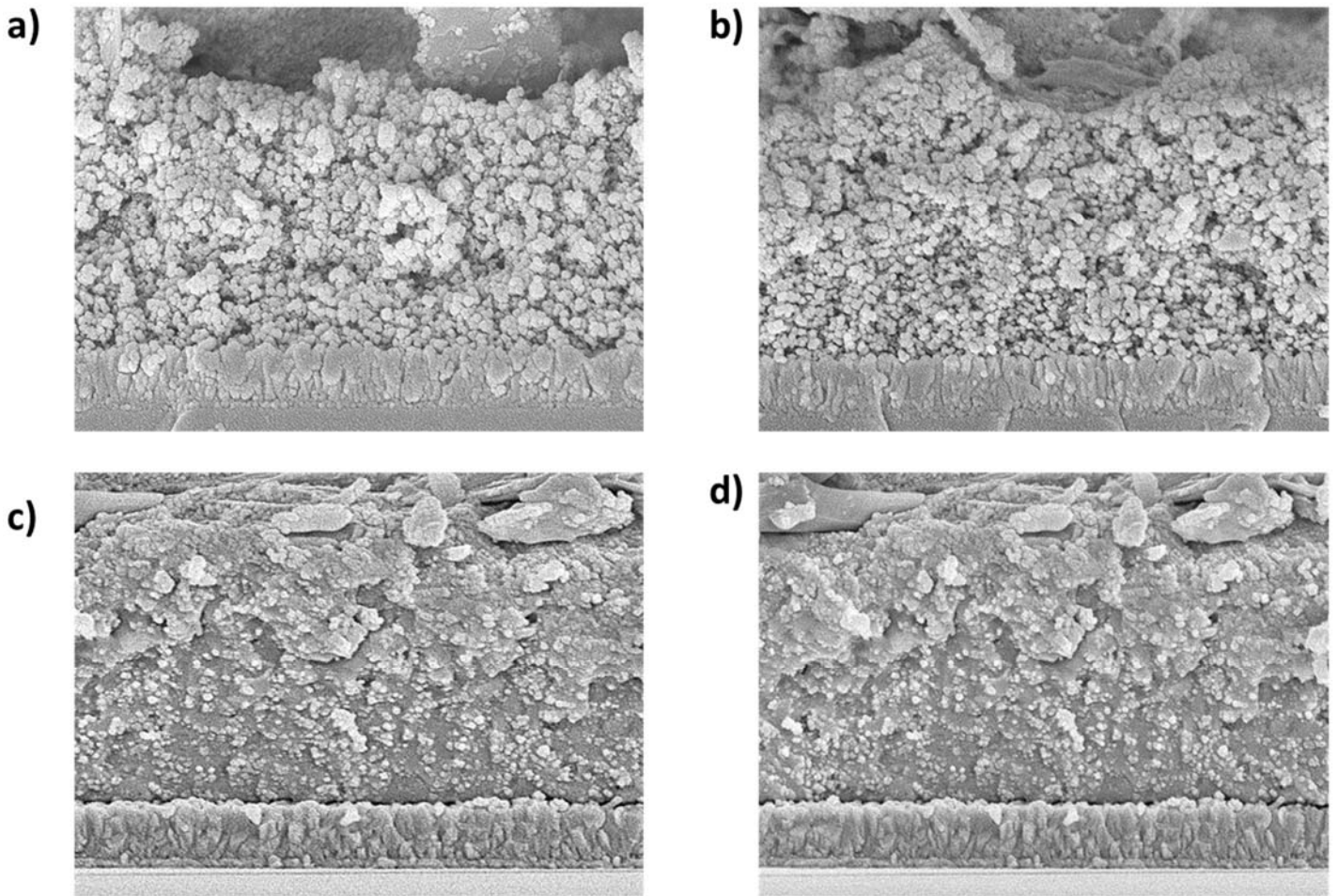


Fig.14 a) SEM Image of reference device without perovskite b) device with Graphene/TiO₂ composite without perovskite c) image of reference device with perovskite d) device with Graphene/TiO₂ composite with perovskite

Device Performance

The devices with active area of 0.7cm² were fabricated to assess the performance of devices with graphene/TiO₂ composite as an ETL. The performance of the PSCs for each device type are reported in Figure 15.

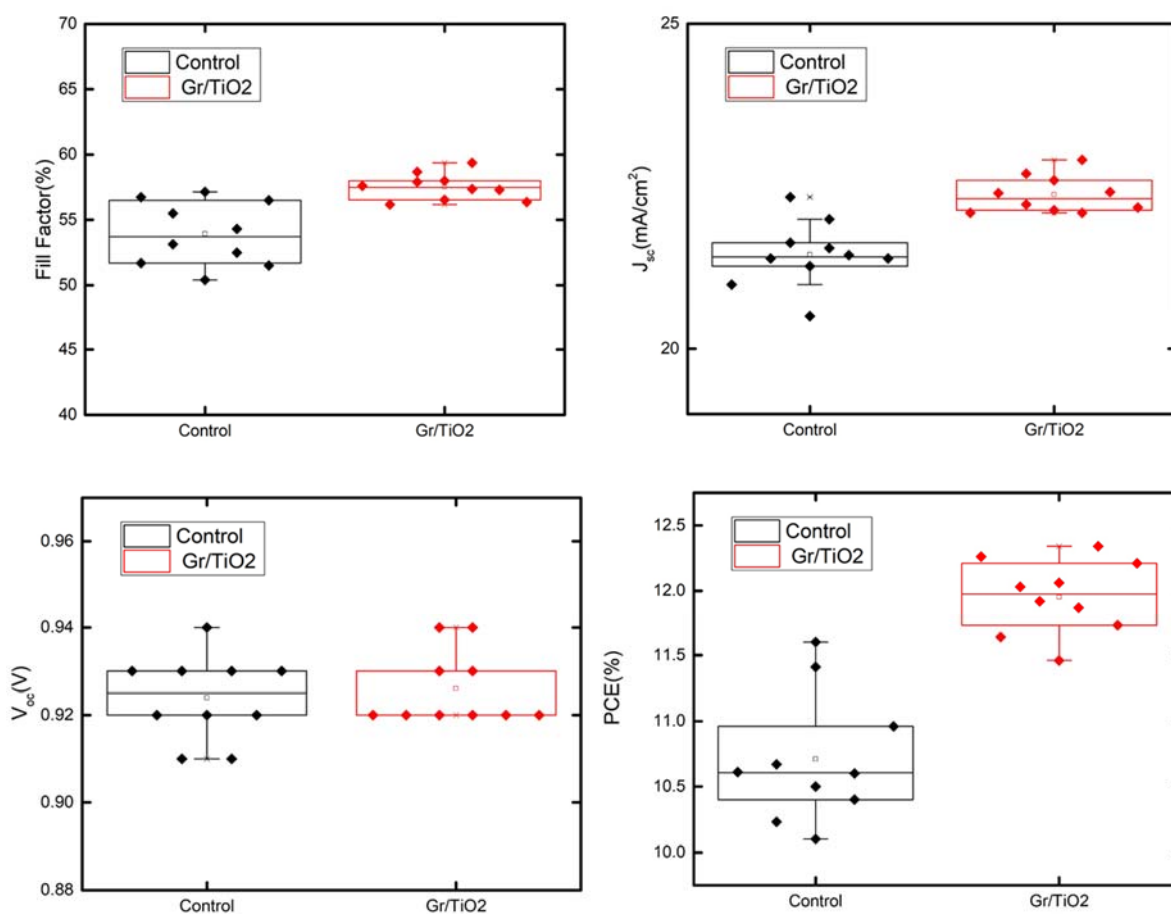


Fig.15 Relative performance parameters and relative standard deviation of 10 PSCs for control and devices with graphene/TiO₂ composite

It can be inferred from the data above that the devices with composite of graphene and TiO₂ performed better relative to the reference cells. The champion cell hit the efficiency over 12% (Fig. 16 b). Insertion of graphene led to a remarkable improvement in J_{sc} and FF. The average FF improved by 5.6% and average J_{sc} by 2.5%. The devices also exhibit negligible hysteresis Fig. 16(c,d).

Parameters	Without Graphene		With Graphene	
	Forward	Reverse	Forward	Reverse
V_{oc} (V)	0.90	0.92	0.92	0.93
J_{sc} (mA/cm ²)	21.22	21.4	22.42	22.64
FF (%)	56.62	54.12	57.6	56.18
PCE (%)	10.83	10.62	12.3	11.89

Table 2 Performance parameters for standard carbon cell and cells with graphene-TiO₂ composite under 1 Sun light illumination.

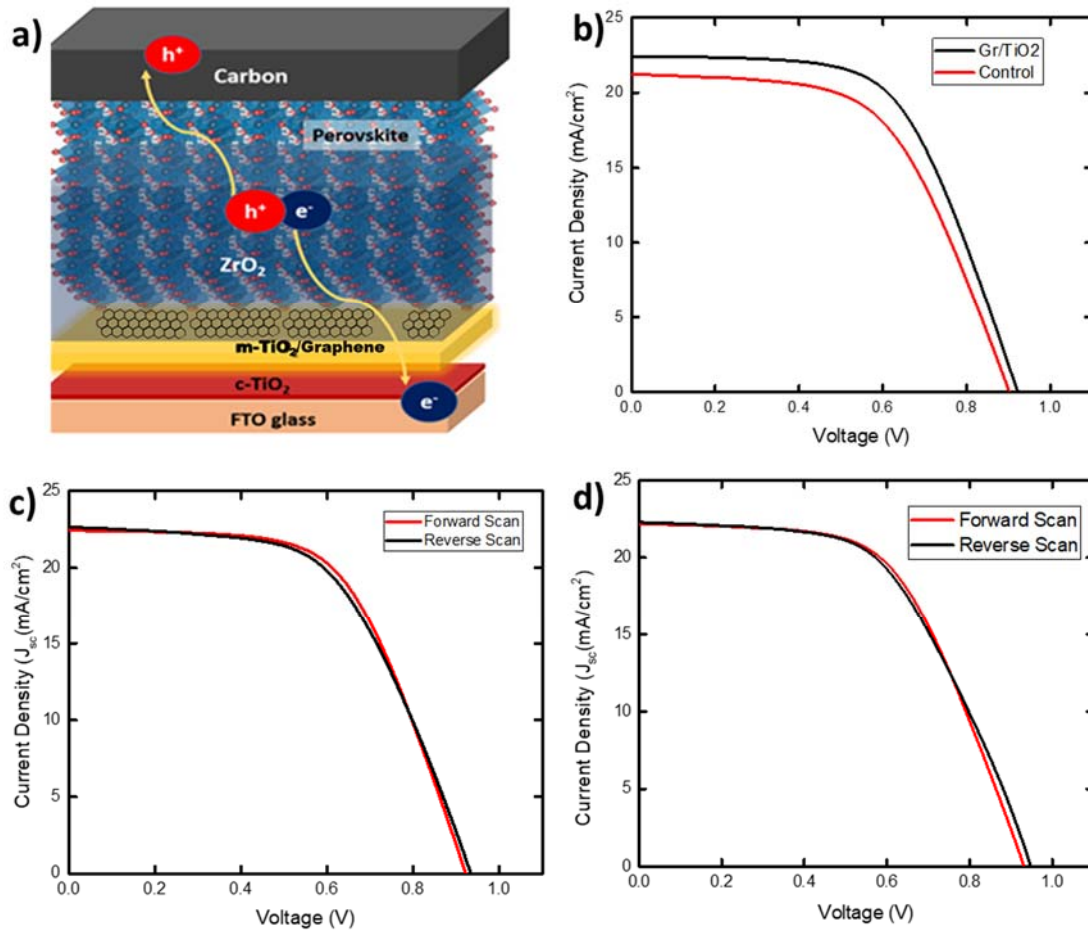


Fig. 16 a) Schematic of complete graphene device b) J-V curve comparing performance of reference with that of graphene devices c) and d) J-V plots showing hysteresis in graphene and reference respectively.

Device Characterization

To investigate the effect on charge transport properties due to graphene insertion, the J_{sc} vs solar irradiation was recorded. This data can provide valuable information about the charge transport within perovskite and charge transport layer.[29] Fig. 17a represents a linear curve, indicative of absence of any trap assisted recombination. It can be noted that the devices with graphene insertion has higher J_{sc} - P_{inc} slope representing better charge transport at perovskite and TiO₂/graphene interface.[30] To record this data the device was kept at short circuit condition and intensity was varied from 0.6 Sun to 1 Sun. To further investigate the improved charge transfer by graphene insertion, photoluminescence spectra was taken. Photoluminescence quenching is shown in Fig. 17b. The red curve represents the peak of MAPI₃ at 764nm corresponding to its bandgap. The PL intensity is strongly quenched by the graphene/TiO₂ charge extraction layer compared to the TiO₂ alone which shows better charge extraction by the incorporation of graphene.

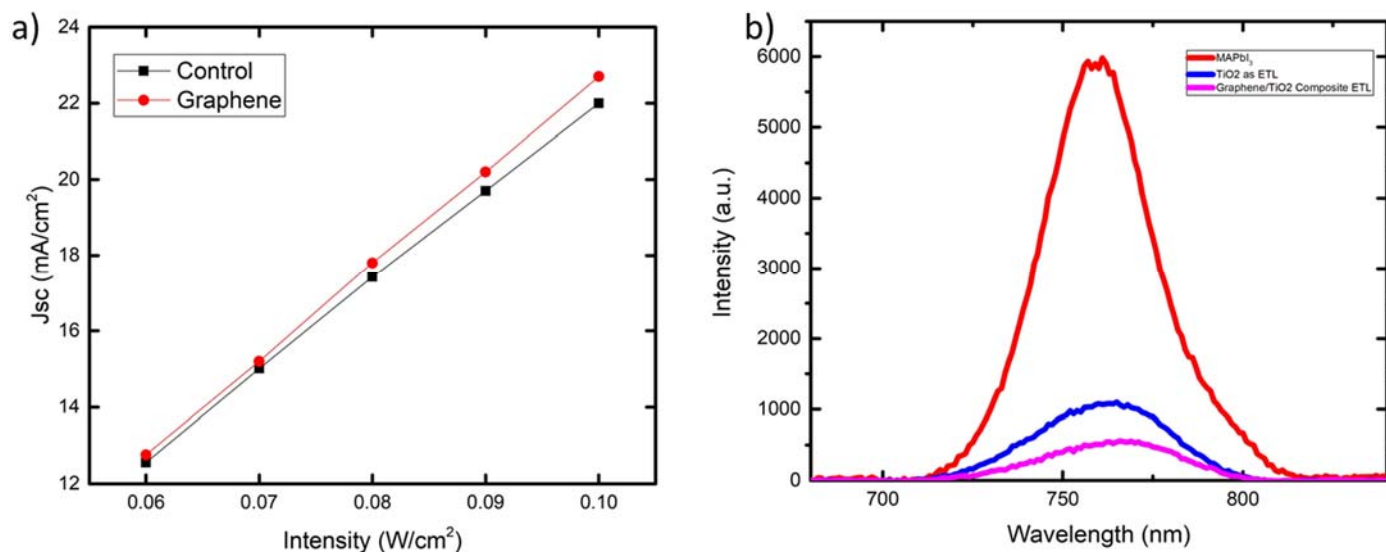


Fig.17 a) J_{sc} vs incident power b) Photoluminescence (PL) spectra of MAPbI₃, TiO₂/MAPbI₃ and Graphene-TiO₂/MAPbI₃

Impedance spectroscopy is widely used tool to probe the charge dynamics at the interface of semiconductor and is often used to study the charge transfer resistance and recombination resistance in PSCs. To confirm the drop in series resistance and charge transfer resistance Impedance spectroscopy was performed. In carbon based PSCs the charge transfer takes place between ETL/perovskite interface and carbon/perovskite interface. The EIS spectra under light shows two semicircle. Each semicircle represents one R-C element. One R-C element is attributed to recombination resistance and the other to charge transfer resistance. The fitted EIS spectra shown in figure 18a compares the charge dynamics of devices with graphene-mTiO₂ relative to the reference cells. The bigger arc corresponds to recombination resistance, value of which is higher in case of graphene-mTiO₂ cells which confirms less recombination in the case of graphene-mTiO₂ devices. The smaller arc corresponds to the charge transfer resistance which shows lesser charge transfer resistance in graphene-mTiO₂ device which justifies the improvement in J_{sc} and FF of graphene incorporated devices. Also, Fig.18b shows the charge transfer resistance at different potential where we further confirm the reduction of charge transfer resistance at different potential. All the measurements were done under 1 Sun illumination. The EIS data was fitted using the circuit shown in Fig. 19

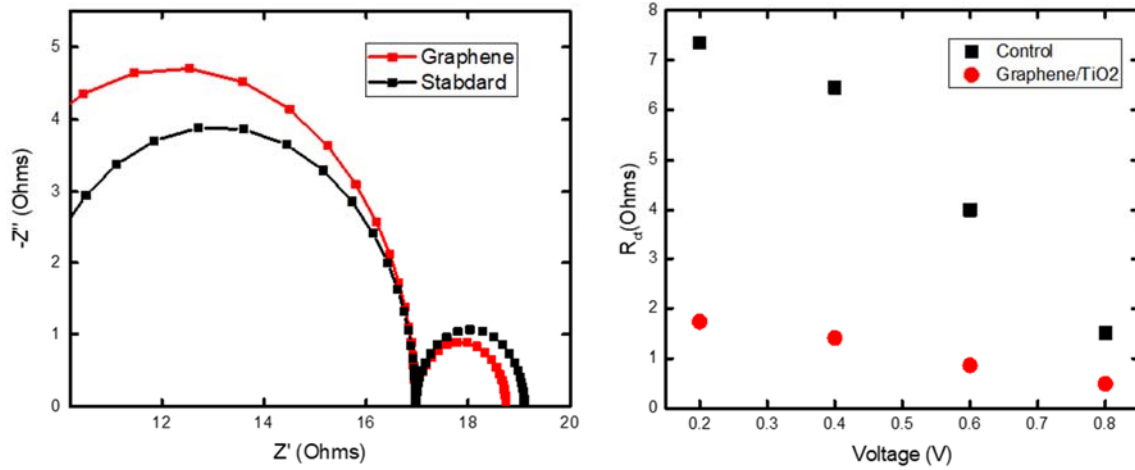


Fig.18 a) Nyquist plot of graphene devices compared with reference cells taken under 1 Sun illumination at 0.4V
b) Charge transfer resistance plotted at different voltage of both the cases.

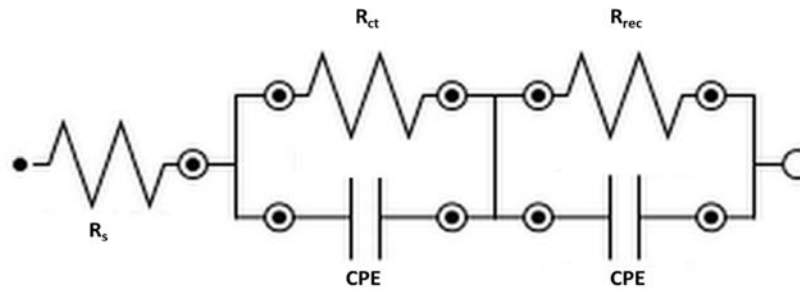


Fig. 19 Equivalent circuit diagram used for the fitting of EIS spectra

Device Stability

To check the stability of fabricated cells at continuous illumination, maximum power point tracking (MPPT) was performed. The voltage at maximum power point was recorded first by performing J-V scan of the cells. The cells were then kept at the recorded voltage under 1 Sun illumination for 20 hours and the current readings were recorded every 10 secs. The PCE was calculated using the following equation:

$$\eta (\%) = \frac{P_{out}}{P_{in}}$$

$$\eta (\%) = \frac{IV}{P_{in}}$$

The obtained data is shown in Fig. 20a. The reference cells showed degradation of 15% to their initial efficiency in 20 hours, while graphene incorporated cells just dropped to only 3% of their initial PCE in the span of 20 hours. This concludes that incorporation of graphene didn't only increase the PCE but stability was also

significantly improved. The reason for this observation is yet to determine and would be a subject for future research work. Observing an excellent stability under illumination we also tested both batch of devices under 85°C at 5% relative humidity. The cells degrades significantly faster and no clear trend was observed while similar degradation rate was noted in both the cases. (Fig. 20b)

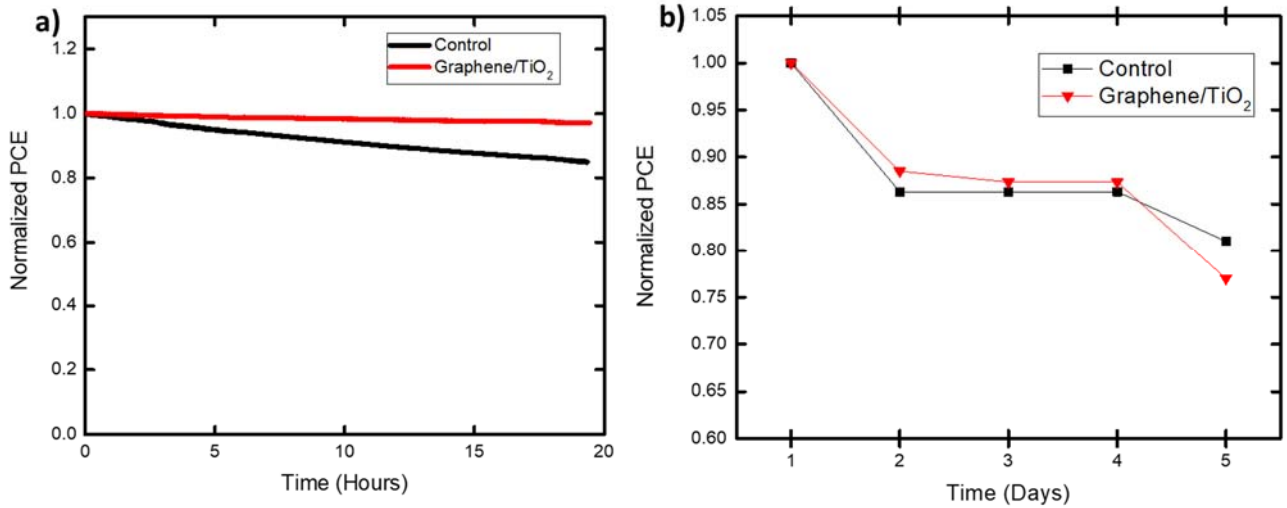


Fig. 20 a) MPPT of reference (V_{max} 0.58V) vs Graphene/TiO₂ (V_{max} 0.63V) cells under 1 Sun illumination b) thermal stability of reference vs Graphene/TiO₂ at 85°C

Large Area Device

Finally we fabricated a large area (70cm²) device to assess the effect of addition of graphene on large area. The respective performance are shown in Fig. 21a.

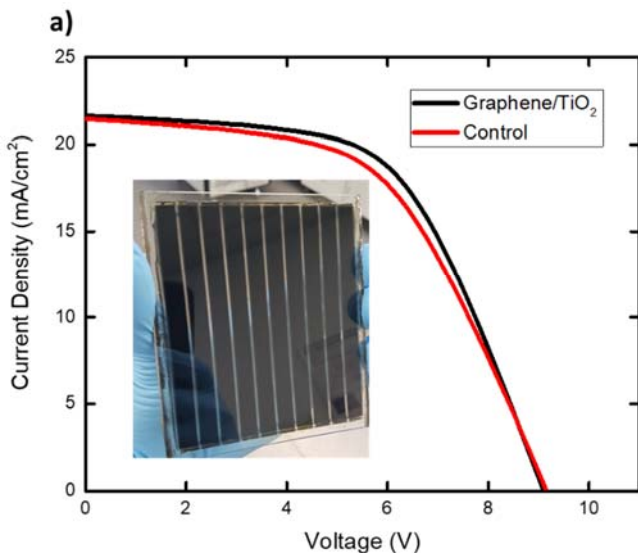


Table 3

Parameters	Without Graphene		With Graphene	
	Forward	Reverse	Forward	Reverse
$V_{oc}(V)$	8.9	9.14	8.83	9.09
$J_{sc}(mA/cm^2)$	20.48	21.4	20.8	21.6
FF (%)	58.78	54.10	60.31	57.25
PCE (%)	10.72	10.61	11.1	11.26

Fig.21 a) J-V plot of 70cm² module of reference and Graphene incorporated devices. Table 3) Performance parameters of 70cm² module for both the cases.

Conclusion

We show the effect of graphene as an additive in ETL to enhance the performance and stability of PSCs. In particular, we have successfully demonstrated the improvement in PCE of small and large area PSCs by using the composite of graphene and TiO₂ as electron transport material. The champion cell performed well over PCE of 12%. EIS measurement and PL measurement revealed the improvement in charge transport properties by the incorporation of graphene. The addition of graphene leads to a significant drop in charge transfer resistance resulting in a significant improvement in FF and recorded J_{sc} as high as 22.7 mA/cm². We performed impedance measurement to quantify the charge transfer resistance and it shows significantly lower charge resistance in the devices with graphene/TiO₂ as ETL. Which concludes that graphene in TiO₂ is helping in boosting the charge extraction from the active layer of perovskite. The presence of graphene in composite was confirmed by Raman spectroscopy. However, the graphene in composite was found to be multilayer graphene. SEM images show no significant change in the morphology of perovskite crystal growth in presence of graphene. Next, we performed the thermal stability and stability under continuous illumination. The devices with graphene composite came out as a clear winner in the battle of MPPT tracking while no improvement was observed in thermal stability. At last we used graphene composite in large area 70cm² module and shown a slight improvement in PCE. Thus we conclude the use of graphene in complete mesoporous architecture for stable and efficient large area PSCs.

References

1. Tsao, J., N. Lewis, and G. Crabtree, *Solar FAQs*. US department of Energy, 2006.
2. Stranks, S.D., et al., *Electron-hole diffusion lengths exceeding 1 micrometer in an organometal trihalide perovskite absorber*. Science, 2013. **342**(6156): p. 341-4.
3. deQuilettes, D.W., et al., *Solar cells. Impact of microstructure on local carrier lifetime in perovskite solar cells*. Science, 2015. **348**(6235): p. 683-6.
4. Xing, G., et al., *Long-range balanced electron-and hole-transport lengths in organic-inorganic CH₃NH₃PbI₃*. Science, 2013. **342**(6156): p. 344-347.
5. Kojima, A., et al., *Organometal halide perovskites as visible-light sensitizers for photovoltaic cells*. Journal of the American Chemical Society, 2009. **131**(17): p. 6050-6051.
6. Yang, W.S., et al., *Iodide management in formamidinium-lead-halide-based perovskite layers for efficient solar cells*. Science, 2017. **356**(6345): p. 1376-1379.

7. Green, M.A., A. Ho-Baillie, and H.J. Snaith, *The emergence of perovskite solar cells*. Nature Photonics, 2014. **8**(7): p. 506-514.
8. Kim, H.-S., et al., *Lead iodide perovskite sensitized all-solid-state submicron thin film mesoscopic solar cell with efficiency exceeding 9%*. Scientific reports, 2012. **2**.
9. Lee, M.M., et al., *Efficient hybrid solar cells based on meso-superstructured organometal halide perovskites*. Science, 2012. **338**(6107): p. 643-647.
10. Etgar, L., et al., *Mesoscopic CH₃NH₃PbI₃/TiO₂ heterojunction solar cells*. Journal of the American Chemical Society, 2012. **134**(42): p. 17396-17399.
11. Ku, Z., et al., *Full printable processed mesoscopic CH₃NH₃PbI₃/TiO₂ heterojunction solar cells with carbon counter electrode*. Sci Rep, 2013. **3**: p. 3132.
12. Zhang, F., et al., *Structure engineering of hole-conductor free perovskite-based solar cells with low-temperature-processed commercial carbon paste as cathode*. ACS applied materials & interfaces, 2014. **6**(18): p. 16140-16146.
13. Duan, M., et al., *Efficient hole-conductor-free, fully printable mesoscopic perovskite solar cells with carbon electrode based on ultrathin graphite*. Carbon, 2017. **120**: p. 71-76.
14. Ku, Z., et al., *A mesoporous nickel counter electrode for printable and reusable perovskite solar cells*. Nanoscale, 2015. **7**(32): p. 13363-13368.
15. Priyadarshi, A., et al., *A large area (70 cm²) monolithic perovskite solar module with a high efficiency and stability*. Energy Environ. Sci., 2016. **9**(12): p. 3687-3692.
16. Mei, A., et al., *A hole-conductor-free, fully printable mesoscopic perovskite solar cell with high stability*. Science, 2014. **345**(6194): p. 295-8.
17. Agresti, A., et al., *Graphene-Perovskite Solar Cells Exceed 18% Efficiency: A Stability Study*. ChemSusChem, 2016. **9**(18): p. 2609-2619.
18. Al-Alwani, M.A., et al., *Dye-sensitised solar cells: Development, structure, operation principles, electron kinetics, characterisation, synthesis materials and natural photosensitisers*. Renewable and Sustainable Energy Reviews, 2016. **65**: p. 183-213.
19. Akihiro Kojima, K.T., Yasuo Shirai, and Tsutomu Miyasaka, *Organometal Halide Perovskites as Visible-Light Sensitizers for Photovoltaic Cells*. J Am Chem Soc, 2009. **2009** (131): p. 6050-6051.
20. Soucase, B.M., I.G. Pradas, and K.R. Adhikari, *Numerical Simulations on Perovskite Photovoltaic Devices*, in *Perovskite Materials-Synthesis, Characterisation, Properties, and Applications*. 2016, InTech.
21. Goldschmidt, V.M., *Die gesetze der krystallochemie*. Naturwissenschaften, 1926. **14**(21): p. 477-485.
22. Tong, X., et al., *High performance perovskite solar cells*. Advanced Science, 2016. **3**(5).
23. Lee, D.-H., et al., *Screen-printed white OLED based on polystyrene as a host polymer*. Current Applied Physics, 2009. **9**(1): p. 161-164.

24. Hsu, R.C., et al., *A reinforcement learning-based maximum power point tracking method for photovoltaic array*. International Journal of Photoenergy, 2015. **2015**.
25. *Solar Cell I-V Characteristic*. Available from: <http://www.alternative-energy-tutorials.com/energy-articles/solar-cell-i-v-characteristic.html>.
26. *Raman Spectroscopy Characterization of Grphene and Graphene Oxide*. Available from: <https://instanano.com/characterization/experimental/raman-graphene/>.
27. Naureen, S., *Top-down Fabrication Technologies for High Quality III-V Nanostructures*. 2013, KTH Royal Institute of Technology.
28. Ferrari, A.C. and D.M. Basko, *Raman spectroscopy as a versatile tool for studying the properties of graphene*. Nature nanotechnology, 2013. **8**(4): p. 235.
29. Zhang, H., et al., *CuGaO2: A Promising Inorganic Hole-Transporting Material for Highly Efficient and Stable Perovskite Solar Cells*. Advanced Materials, 2017. **29**(8).
30. Katz, E., et al., *Light intensity dependence of External Quantum Efficiency of fresh and degraded organic photovoltaics*. Solar Energy Materials and Solar Cells, 2016. **144**: p. 273-280.